

A finite element analysis of a new design of a biomimetic shape memory alloy artificial muscle

Moez Ben Jaber^{*1,2}, Mohamed A. Trojette³ and Fehmi Najjar¹

¹*Systems and Applied Mechanics Research Laboratory, Tunisia Polytechnic School, University of Carthage, B.P. 743, La Marsa 2078, Tunisia*

²*National Engineering School of Tunis, University of El-Manar, BP 37, Le Belvédère 1002 Tunis, Tunisia*

³*College of Sciences and Techniques of Tunis, University of Tunis, BP 56, 5 Avenue Taha Hussein, Bâb Manara, Tunis, Tunisia*

(Received July 14, 2014, Revised November 30, 2014, Accepted December 29, 2014)

Abstract. In this work, a novel artificial circular muscle based on shape memory alloy (S.M.A.) is proposed. The design is inspired from the natural circular muscles found in certain organs of the human body such as the small intestine. The heating of the prestrained SMA artificial muscle will induce its contraction. In order to measure the mechanical work provided in this case, the muscle will be mounted on a silicone rubber cylindrical tube prior to heating. After cooling, the reaction of the rubber tube will involve the return of the muscle to its prestrained state. A finite element model of the new SMA artificial muscle was built using the software "ABAQUS". The SMA thermomechanical behavior law was implemented using the user subroutine "UMAT". The numerical results of the finite element analysis of the SMA muscle are presented to show that the proposed design is able to mimic the behavior of a natural circular muscle.

Keywords: shape memory alloy; bioinspiration; biomimetic; new design; artificial muscle; finite element analysis

1. Introduction

Shape memory alloys (SMA) are characterized by a special thermomechanical behaviour (Patoor and Berveiller 1994, Otsuka and Wayman 1999). After an appropriate thermomechanical treatment, this alloy can be deformed in appearance of a plastic manner and retrieve its original shape after a simple few degrees heating. If during heating, it is prevented from returning to its original shape it could develop a substantial force. This behaviour is the result of a solid–solid phase transformation known as martensitic transformation (Lu and Weng 1994, Orgéas and Favier 1998). As the temperature varies, the SMA microstructure shifts between two stable states, namely, martensite, at low temperature, and austenite, at high temperature.

Several researchers have attempted to exploit this force in the design of new small actuators, commonly known as artificial muscles (Leary *et al.* 2013, Nespoli *et al.* 2010, Madden *et al.* 2004, Rediniotis and Lagoudas 2001) that have the advantage to produce a high force/volume ratio. Among these researchers one can cited Bundhoo and Park (2005) who proposed a biomimetic

*Corresponding author, Dr., E-mail: moez.jaber@enit.rnu.tn

approach to prosthetic hand design that use SMA wire as a driven tendon directly attached to the finger structure, in a manner similar to the natural tendons and muscles. Luo *et al.* (2005) also developed an artificial anal sphincter that consists of two all-round shape memory alloy plates and heaters attached to the SMA plates. The SMA artificial sphincter could be fitted around intestines, performing an occlusion function at body temperature and a release function upon heating. Another example of such artificial muscle is the one presented by Mascaro *et al.* (2003) where SMA wires are embedded within artificial “blood vessels”. Electric current passed in SMA wire and fluid flowing through vessels allows control of wires temperature resulting in control of the contraction/extension of the SMA wires within the compliant vessels. More examples of SMA artificial muscle can be found in literature (Doroftei and Stirbu 2014, Furst *et al.* 2013, Hartl *et al.* 2010).

In this paper, we propose a new design of artificial muscle based on shape memory alloy. This new design mimics the mode of actuation of natural circular muscles which are found in the small intestine (Fig. 1).

In combination with longitudinal muscles, circular muscles circulate substances in the intestine (Fig. 2).

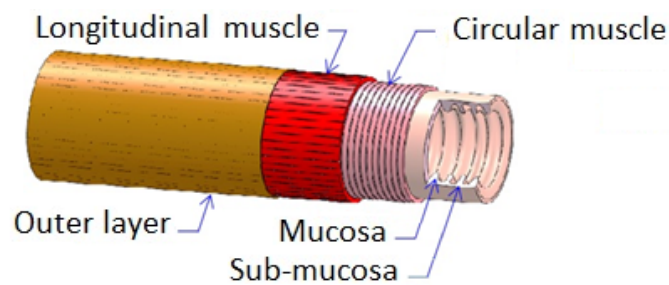


Fig. 1 Circular and longitudinal muscles present in the small intestine

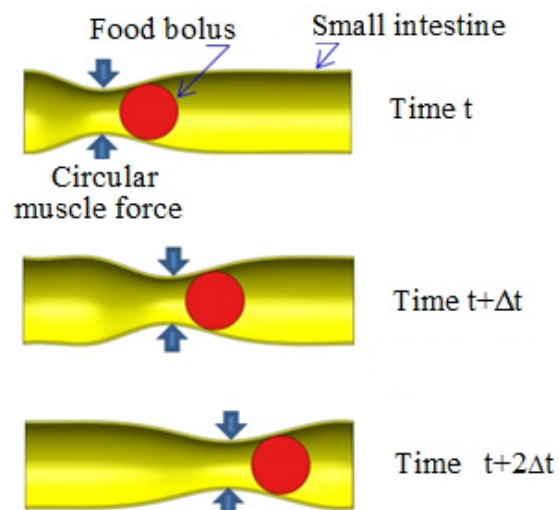


Fig. 2 Actuation mode of circular muscles in a digestive tube to move substances

However, unlike longitudinal muscles, which usually produce longitudinal tensile forces, circular muscles, which are tied to inner layer of the digestive tube, apply radial contraction forces.

The proposed novel design consists of corrugated nickel-titanium (Ni-Ti or nitinol) SMA wire, which will be mounted on a rubber tube (Fig. 3).

The artificial muscle is obtained by folding at 180 degrees of the SMA wire, followed by the bending step obtaining the circular shape. . Given the difficulty of welding of this type of alloy, the connection of the two wire ends can be achieved by using a small clamp ring. Another fabrication technique of such muscle is obtained by laser cutting of a thin SMA tube similar to the case of some coronary stent. The obtained cross section of the muscle is rectangular instead of being circular. After obtaining the desired shape the material must undergo a specific thermomechanical treatment called “training” process to control geometric and mechanical properties.

The basic idea behind this design is to start by expanding the radius of the SMA artificial muscle at the ambient temperature. After unloading, the muscle will retain a permanent deformation. Next, the muscle will be mounted on a silicone rubber tube and then heated by Joule effect using electric current. The recovery of the SMA muscle to its initial shape by memory effect will be stopped by the rubber tube. This results in significant contraction force applied by the muscle on the contact surface with the rubber tube, which induces its elastic deformation. Then, switching off the electric current, the SMA recover its initial ambient temperature and the elastic restoring force of the tube pushes back the muscle to its initial deformed shape.

Thanks to the advantages that the proposed design offers, such as compact size, many potential applications in various fields can be proposed. In biomechanics, for example, the proposed SMA muscle can be used in the design of a new artificial valves and sphincters of various kinds (anal sphincter, vesical sphincter, sphincter of the pylorus...). Biomimetic artificial intestine is another example of application based on this new SMA muscle in order to replace parts of cancer-affected intestine for example. MEMS micropump can also be a one of the areas of possible application of this product because of the important density force that it is able to provide. It can also be used as actuator for robots imitating the movement of earthworms.

The objective of this work is to numerically validate the performances and actuation conditions of the newly proposed artificial muscle design. In what follows the SMA constitutive model used to simulate the SMA artificial muscle is described in Section 2. The finite element model of the muscle and its thermomechanical loading trajectory are presented in Section 3. Finally, the numerical results with discussion and interpretation are documented in Section 4. Finally, these are followed by concluding remarks in Section 5.

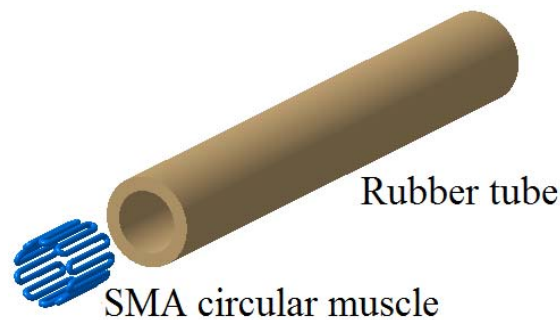


Fig. 3 The design of the SMA artificial circular muscle

2. SMA Constitutive model

To reproduce the shape memory behaviour, we use the SMA constitutive model originally proposed by Ben Jaber (2008). Here a summary of this constitutive model and its numerical implementation are presented. Some modifications will be introduced to the formulation of this constitutive law to improve and simplify the start detection of phase transformation. Another modification that will be described is about the equation of the equivalent Young's modulus.

Given that a beam element was used for the modelling of the artificial muscle, only axial and transverse stress and strain components will be considered as non-zero, hence

$$\boldsymbol{\sigma} = \begin{pmatrix} \sigma \\ \tau \end{pmatrix} \quad (1)$$

$$\boldsymbol{\varepsilon} = \begin{pmatrix} \varepsilon \\ \gamma \end{pmatrix} \quad (2)$$

Two coupled constitutive laws are considered: a thermomechanical and a kinetic laws.

2.1 Thermomechanical law

Since the SMA elastic strain is small compared to the transformation strain, the classical rate-additive hypoelastic plasticity formulation is adopted (De Souza Neto 2011). This approach consists of an additive decomposition of the total rate of deformation $\dot{\boldsymbol{\varepsilon}}$ into an elastic part $\dot{\boldsymbol{\varepsilon}}_{el}$ and a transformation part $\dot{\boldsymbol{\varepsilon}}_{tr}$

$$\dot{\boldsymbol{\varepsilon}} = \dot{\boldsymbol{\varepsilon}}_{el} + \dot{\boldsymbol{\varepsilon}}_{tr} \quad (3)$$

The Jaumann rate of Cauchy stress is governed by the thermomechanical law

$$\dot{\boldsymbol{\sigma}} = \mathbf{R}(\dot{\boldsymbol{\varepsilon}} - \dot{\boldsymbol{\varepsilon}}_{tr}) + \dot{\mathbf{R}}(\boldsymbol{\varepsilon} - \boldsymbol{\varepsilon}_{tr}) + \mathbf{k}\dot{T} + \dot{\mathbf{k}}(T - T_{ref}) \quad (4)$$

where T and T_{ref} are, respectively, the actual temperature and initial temperature, \mathbf{k} denotes the thermal modulus vector and \mathbf{R} is the elastic rigidity tensor.

The effective Young modulus E during martensitic transformation is calculated in terms of the martensite volume fraction using the Reuss model (Brinson and Huang 1996).

$$\frac{1}{E} = \frac{\xi}{E_M} + \frac{1-\xi}{E_A} \quad (5)$$

where E_M and E_A are, respectively, the martensite and the austenite Young's moduli.

This equation replaces the Voigt approximation (Brinson and Huang 1996) of the effective Young's modulus used previously by Ben Jaber *et al.* (2008) to overcome the discrepancy between the model response and the real behaviour of the SMA in case Young's moduli E_A and E_M are very different.

The initial formulation of the equivalent Young's modulus equation is

$$E = \xi E_M + (1 - \xi) E_A \quad (6)$$

To capture the phase transformation effects, the rate of deformation due to martensitic transformation $\dot{\boldsymbol{\varepsilon}}_{tr}$ is given by

$$\dot{\boldsymbol{\varepsilon}}_{tr} = \begin{cases} \dot{\xi} \varepsilon_{tr}^{max} \frac{\sigma}{\sqrt{\sigma^2 + 3\tau^2}} & \text{if } \dot{\xi} > 0 \\ \dot{\xi} \varepsilon_{tr} & \text{if } \dot{\xi} < 0 \end{cases} \quad (7)$$

where $\dot{\xi}$ is the volume fraction change of detwinned martensitic phase and ε_{tr}^{max} is the maximum uniaxial transformation strain.

2.2 Kinetics law

The kinetic law serves to determine the evolution of the phase state for a given strain and temperature increments. One seeks to determine the rate of change $\dot{\xi}$ in the volume fraction of detwinned martensite along with the rate of transformation strain $\dot{\boldsymbol{\varepsilon}}_{tr}$. It is worth noting here that in classic SMA constitutive law (Lagoudas 2000) these rates are computed as a function of temperature and stress evolution by using the classic SMA phase diagram shown in Fig.4. In the martensitic volume fraction we consider only a detwinned martensite because it is the only state that contributes to transformation deformation.

In Fig. 4 the following notations have been used:

- A: austenite
- M^t : twinned martensite
- M^d : detwinned martensite
- σ_s^{AM} : A, M^t to M^d transformation start stress
- σ_f^{AM} : A, M^t to M^d transformation finishing stress
- $\sigma_{s\ cr}^{AM}$: A, M^t to M^d critical transformation start stress
- $\sigma_{f\ cr}^{AM}$: A, M^t to M^d critical transformation finishing stress
- σ_s^{MA} : M^t , M^d to A transformation start stress
- σ_f^{MA} : M^t , M^d to A transformation finishing stress
- M_s : A to M^t transformation start temperature
- M_f : A to M^t transformation finishing temperature
- A_s : M^t , M^d to A transformation start temperature
- A_f : M^t , M^d to A transformation finishing temperature
- C_{AM} : A, M^t to M^d transformation band slope
- C_{MA} : M^t , M^d to A transformation band slope

Since the strain tensor is generally determined first by a finite element method, in the proposed approach one needs to propose a suitable transformation corrector algorithm in order to compute the stress increment.

For the constitutive law used in this work the rate of change in the volume fraction of detwinned martensite $\dot{\xi}$ and the rate of transformation strain $\dot{\boldsymbol{\varepsilon}}_{tr}$ are computed by using the modified phase diagram shown in Fig. 5 (Ben Jaber *et al.* 2008).

In the modified diagram the ε -axis corresponds to the axial strain for one-dimensional behaviour. In three dimensions, this strain parameter is interpreted as an equivalent strain ε_{eq} . In the case of beam element, and when Poisson's effect is neglected, ε_{eq} is defined as (Ben Jaber *et al.* 2008)

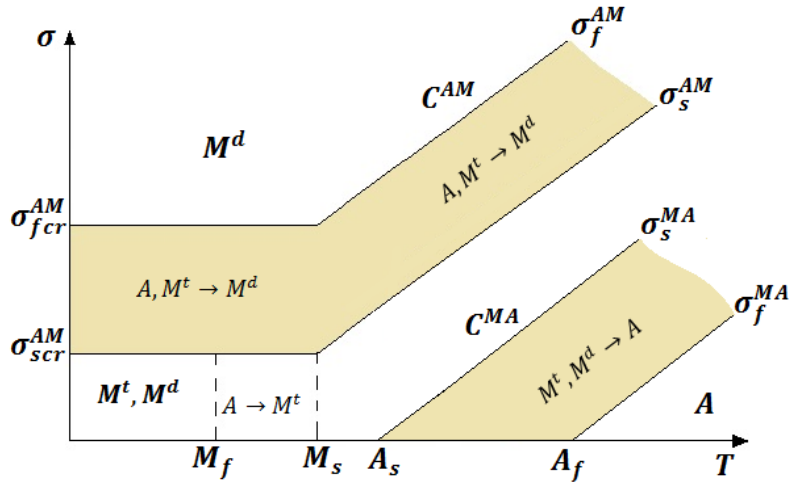


Fig. 4 Phase diagram

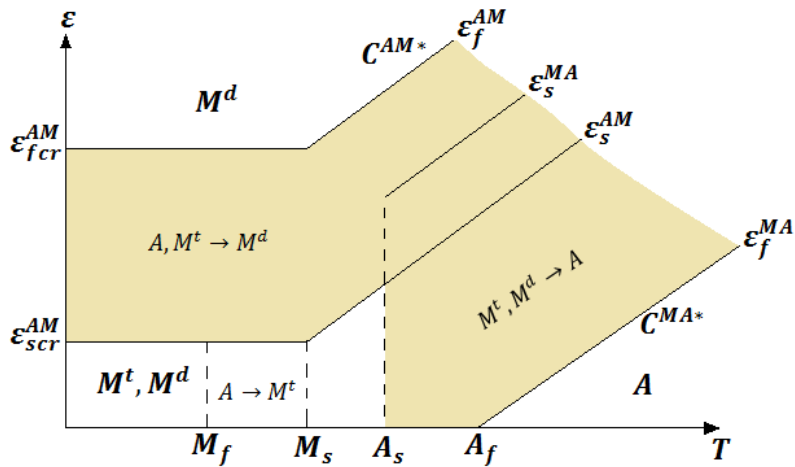


Fig. 5 Modified phase diagram

$$\epsilon_{eq} = \sqrt{\epsilon^2 + \frac{3}{4}\gamma^2} \tag{8}$$

The parameters for this diagram are deduced from those used in the classic phase diagram as follows

$$C^{AM*} = \frac{C^{AM}}{E} \tag{9}$$

$$C^{MA*} = \frac{C^{MA}}{E} \tag{10}$$

$$\varepsilon_{scr} = \varepsilon_{tr eq} + \frac{\sigma_{scr}}{E} \tag{11}$$

$$\varepsilon_{fcr} = \varepsilon_{tr}^{max} + \frac{\sigma_{fcr}}{E} \tag{12}$$

where

$$\varepsilon_{tr eq} = \sqrt{\varepsilon_{tr}^2 + \frac{3}{4}\gamma_{tr}^2} \tag{13}$$

Let ε and T_0 denote the current strain and temperature. Next, we define:

- the strain ε_s^{AM} indicating the beginning of the transformation band A–M

$$\varepsilon_s^{AM} = \begin{cases} \varepsilon_{scr} + C_M^*(T_0 - M_s) & si \ T_0 \geq M_s \\ \varepsilon_{scr} & si \ T_0 \leq M_s \end{cases} \tag{14}$$

- the strain ε_f^{AM} indicating the end of the transformation band A–M

$$\varepsilon_f^{AM} = \begin{cases} \varepsilon_{fcr} + C_M^*(T_0 - M_s) & si \ T_0 \geq M_s \\ \varepsilon_{fcr} & si \ T_0 \leq M_s \end{cases} \tag{15}$$

- the strain ε_s^{MA} indicating the beginning of the transformation band M–A

$$\varepsilon_s^{MA} = \varepsilon_{tr eq} + C_A^*(T_0 - A_s) \tag{16}$$

- the strain ε_f^{MA} indicating the end of the transformation band M–A

$$\varepsilon_f^{MA} = C_A^*(T_0 - A_f) \tag{17}$$

To determine whether the martensitic transformation will occur or not, we define the control function ε^{AM} , revealing the current status, as follows

$$\varepsilon^{AM} = \begin{cases} \varepsilon_{eq} + C^{AM*}(T - T_0) & si \ T_0 \geq M_s \\ \varepsilon^{AM} = \varepsilon_{eq} & si \ T_0 < M_s \end{cases} \tag{18}$$

The transformation of austenite to martensite occurs if the following conditions are satisfied

$$\varepsilon_s^{AM} < \varepsilon^{AM} < \varepsilon_f^{AM}, \dot{\varepsilon}^{AM} > 0 \text{ and } 0 < \xi < 1 \tag{19}$$

The rate of the volume fraction of martensite is defined by the equation

$$\dot{\xi} = (1 - \xi) \frac{\dot{\varepsilon}^{AM}}{(\varepsilon_f^{AM} - \varepsilon_s^{AM})} \tag{20}$$

In the case of inverse transformation, we define the control function ε^{MA} as

$$\varepsilon^{MA} = C^{MA*}(T - T_0) + \varepsilon_{eq} \tag{21}$$

The inverse transformation of martensite to austenite occurs when the following conditions are satisfied

$$\varepsilon_s^{MA} > \varepsilon^{MA} > \varepsilon_f^{MA}, \dot{\varepsilon}^{MA} < 0 \text{ and } \xi > 0 \tag{22}$$

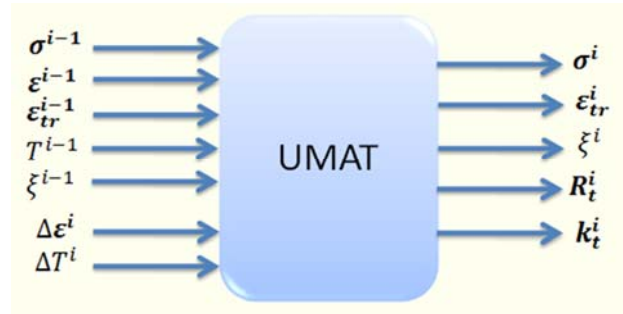


Fig. 6 Input and output of the user subroutine “UMAT”

In this case, the variation of the volume fraction of martensite is defined by the equation

$$\dot{\xi} = -\xi \frac{\dot{\varepsilon}^{MA}}{(\varepsilon_f^{MA} - \varepsilon^{MA})} \quad (23)$$

2.3 Numerical implementation of the SMA constitutive model

The SMA constitutive model described above was introduced in the commercial finite element software "Abaqus" using the user subroutine "UMAT". "Fortran" language is used to implement the proposed customized constitutive model. In this procedure, for each iteration i , the strain tensor, stress tensor and temperature at the previous iteration as well as the increments of temperature and strain tensor at the current iteration are provided. The procedure "UMAT" calculates the new stress tensor, tangent stiffness tensor and thermal coefficient tensor for the current iteration (see Fig. 6). The user can also input a number of additional internal variables (state variables) to calculate, for example in our case, the evolution of the volume fraction of martensite and the transformation strain tensor.

For the implementation of the SMA thermo-mechanical constitutive model, an elastic predictor–transformation corrector return-mapping algorithm is adopted. This algorithm consists of two stages:

(i) The elastic stage, which aims at determining whether or not phase transformation is to occur, and giving the directions of evolution of transformation in case it does take place.

(ii) The stage of transformation correction in which the transformation strain tensor, the volume fraction of martensite and the stress tensor, relative to the total strain found in stage (i), are updated.

The modified Newton–Raphson method (Dhatt *et al.* 1984, Zienkiewics 2005) is adopted here by letting the elastic stiffness tensor, evaluated at each iteration, be used to calculate the element stiffness matrix. This choice allows us to avoid a complex calculation of the tangent stiffness tensor and thus enables a simple implementation of our constitutive model.

In order to verify the validity of the elaborated numerical model to reproduce the main effects of shape memory alloys, two numerical tests have been conducted, namely the superelastic effect test and the one-way shape memory effect test. Table 1 indicates the material properties chosen arbitrarily for these numerical tests. The effects of thermal expansion will be neglected because they are very small compared to the deformations due to the martensitic transformation.

Table 1 Material properties of the artificial muscle

Ni-Ti Shape Memory Alloy Characteristics	Values
E_A	$8 \cdot 10^4$ MPa
E_M	$3 \cdot 10^4$ MPa
ϑ_A	0.43
ϑ_M	0.43
M_s	15°C
M_f	5°C
A_s	25°C
A_f	35°C
ϵ_{tr}^{max}	0.06
σ_{scr}^{AM}	100 MPa
σ_{fcr}^{AM}	170 MPa
C^{AM}	5 MPa °C ⁻¹
C^{MA}	5 MPa °C ⁻¹

Both tests are applied on a straight beam of length 200 mm with circular cross section of diameter 10 mm initially assumed in the austenitic state. In these tests, the SMA beam is subjected to two different thermomechanical uniaxial loading trajectories:

The first case of loading will highlight the ability of the numerical model to describe the superelastic response of the material. Since this effect will occur only for temperatures above A_f , the initial temperature of the beam is fixed at a value equal to 37°C. The load is applied uniaxially until complete martensitic transformation is obtained. The material is then discharged to a zero stress, recovering thereby the entire transformation deformation.

Fig. 7 presents the stress–strain curve from a superelastic tension test. It is observed that the material recovers the original shape after unloading, reproducing a superelastic behavior for $T > A_f$.

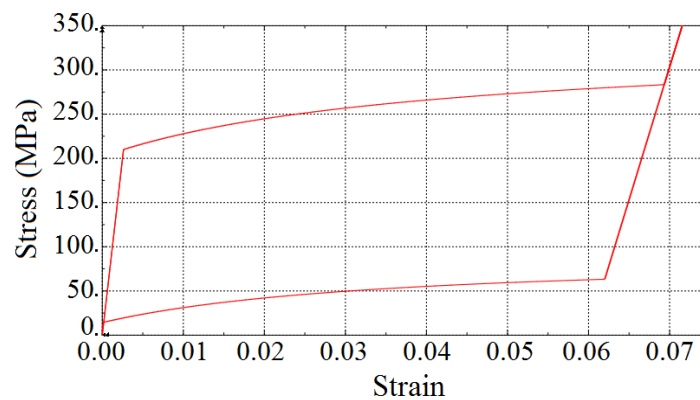


Fig. 7 The stress–strain curve from a superelastic test

The second loading case will highlight the ability of the numerical model to describe shape memory effect of the material. Initially, the material temperature is equal to 37°C (above A_f). Firstly it is cooled to a temperature of 20°C (under the temperature A_s). Next, a tensile force is applied until full martensitic transformation is achieved. The material is then unloaded to zero stress. Finally, the material is heated again to a temperature of 37°C above A_f , which results in reverse phase transformation and recovery of the transformation strain.

Fig. 8 shows the evolution of deformation with stress and temperature. It shows that the model is able to reproduce the characteristic behaviour of the shape memory effect.

3. Finite element analysis of the SMA artificial muscle

The geometrical model of the artificial muscle is presented in Fig. 9(a). The muscle is of diameter 10 mm, 10 mm length and the wire cross-section diameter is 1 mm. The radius of the rounded section that joining the straight parts is 1,5 mm. The number of plies in the muscle is equal to 20.

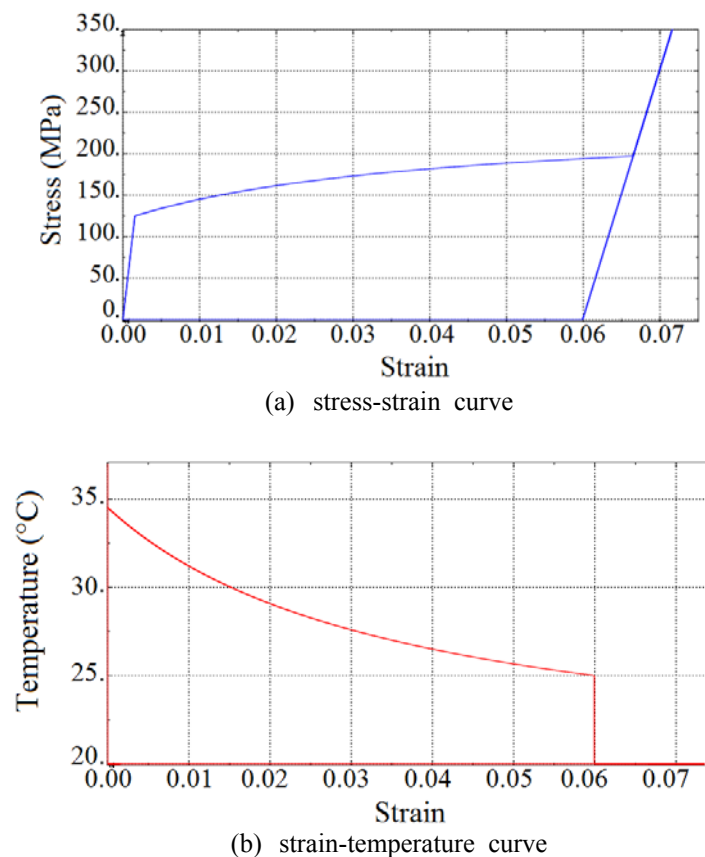


Fig. 8 The stress-strain and strain-temperature curves from a shape memory effect test



Fig. 9 The geometrical model of the artificial muscle

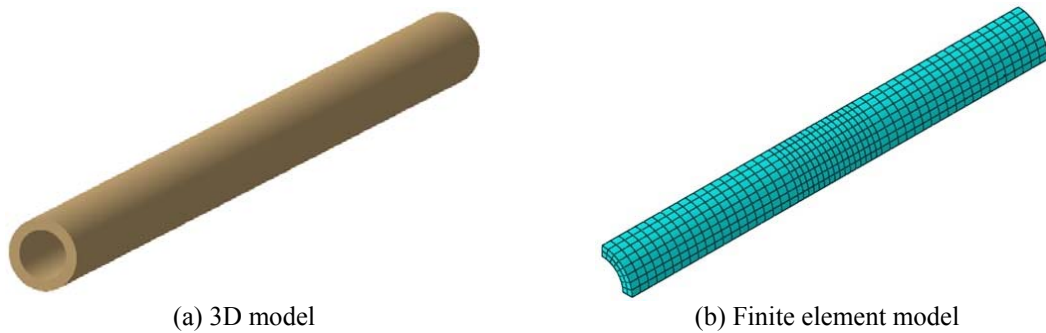


Fig. 10 The geometrical model of the rubber tube

A 3D wireframe model is used for the finite element model of the muscle. Given the symmetry of the geometry, only one quarter of the model will be introduced. The mesh of the artificial muscle is composed of a 3-node quadratic beam "B32" (Fig. 9(b)).

The rubber tube was implemented using a solid model (Fig. 10(a)). It is modelled by a quarter of a hollow cylinder with an outer diameter of 14.5 mm, an inner diameter of 10 mm and length of 100 mm. The mesh of the rubber tube is based on a 20-node quadratic brick hybrid element "C3D20H".

The mesh size of the portion in contact with the muscle was refined (Fig. 10(b)).

A Mooney-Rivlin model was used to simulate the silicone rubber behaviour assumed to be incompressible hyperelastic material. Equation 24 (Ali *et al.* 2010) shows the 2 parameter Mooney-Rivlin model which gives the strain energy potential function W in terms of deviatoric strain invariants \bar{I}_1 and \bar{I}_2 and the material constants C_{01} and C_{10} .

$$W = C_{01}(\bar{I}_2 - 3) + C_{10}(\bar{I}_1 - 3) \quad (24)$$

The Mooney Rivelin coefficients for the silicone rubber tube are chosen as follows

$$C_{10}=0.148 \text{ MPa and } C_{01}= -0.02 \text{ MPa.}$$

For the material properties of the SMA muscle we have used the same values described earlier in Table 1.

The different steps of thermomechanical loading of the artificial muscle are as follows:

- First step (Extension): To mount the muscle on the tube, it will first be deformed to increase its radius initially lower than the outer surface of the tube. The various nodes of the muscle will undergo an imposed radial displacement of 3.5 mm. This deformation is performed for a temperature equal to 20°C that is to say lower than the austenite transformation start temperature ($T < A_s$). This choice of temperature is intended to create a permanent deformation due to the martensitic transformation, which will be retained by the muscle after unloading.
- Second step (Unloading): The radial displacement imposed to the muscle will be disabled to activate the unloading.
- Third step (Assembly): Axial displacement is imposed on the muscle to mount it around the tube.
- Step four (Heating): The temperature of the muscle is increased up to 90°C in order to return the shape memory back to its initial state and therefore creating a contraction of the muscle around the rubber tube.
- Step Five (Cooling): This step was added to check if the elastic restoring force of the rubber tube is sufficient to recover the muscle to initial extended shape when room temperature (20°C) is applied (switching off the electrical current).
- Steps Six to Nine (Cyclic heating and cooling): To verify repeatability of the muscle behaviour it will be subjected to a cyclic heating and cooling between the room temperature and a temperature equal to 90°C.

The contact between the tube and the artificial muscle was introduced by the definition of a "node to surface" interaction whose surface was the outer surface of the tube and nodes were those constituting the entire muscle. The surface of the tube is considered as "master" while the nodes of muscle will be considered as "slave." The penalty method was chosen to solve the contact problem. No slip will be considered after the contact between the muscle and the tube is established.

4. Results and discussion

The Figs. 11(a)-11(c) show deformed shape and von-Mises stress distribution in the artificial circular muscle respectively after loading and unloading.

At the end of the unloading step (Fig. 11(c)) a permanent deformation was maintained by the SMA which has permitted to preserve the inner radius of the artificial muscle larger than that of the outer surface of the rubber tube. This will allow both parts to be assembled.

It is important to verify that the von-Mises stress in both parts remain below an acceptable limit. In the same time, the stress in the shape memory alloy must be enough to initiate martensitic transformation and produce enough martensite to produce the required deformation of the muscle. This compromise can be achieved by properly selecting the dimensions of the muscle like the cross section diameter of SMA wire, radius of folds and number of folds, etc.

In this study, the considered SMA yield stress is equal to 350 MPa, which is an acceptable value compared with values reported in the literature (Paivo *et al.* 2005, Lagoudas and Entchev 2003). As for the silicone rubber, the maximum value of von Mises stresses found is very small (about 0.06 MPa) which is certainly acceptable by this type of material.

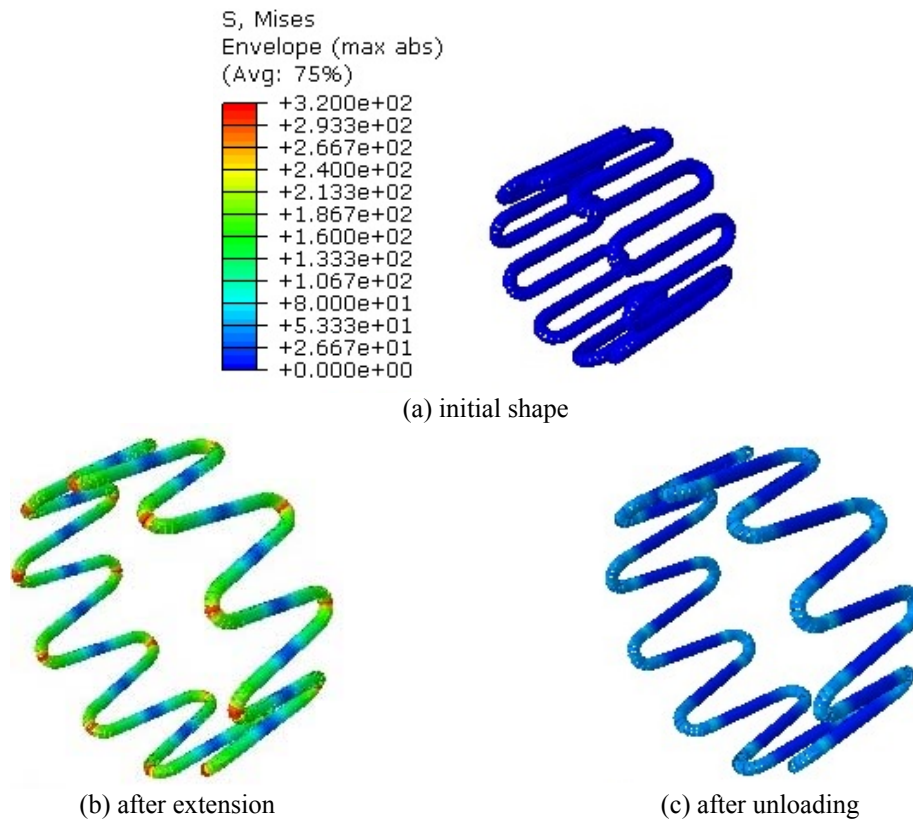


Fig. 11 Deformed shape and von-Mises stress distribution (in MPa) in the artificial circular muscle

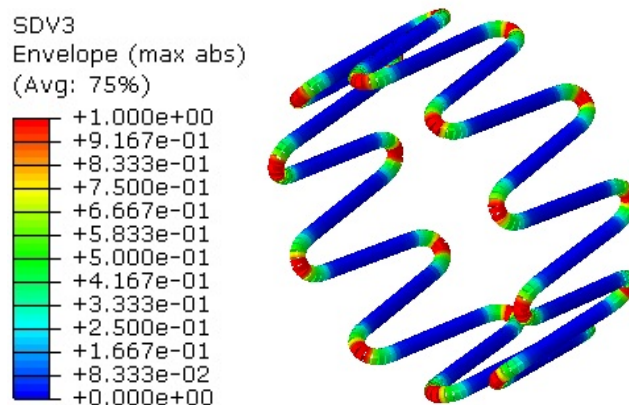


Fig. 12 The distribution of the volume fraction of martensite in the SMA muscle after unloading step

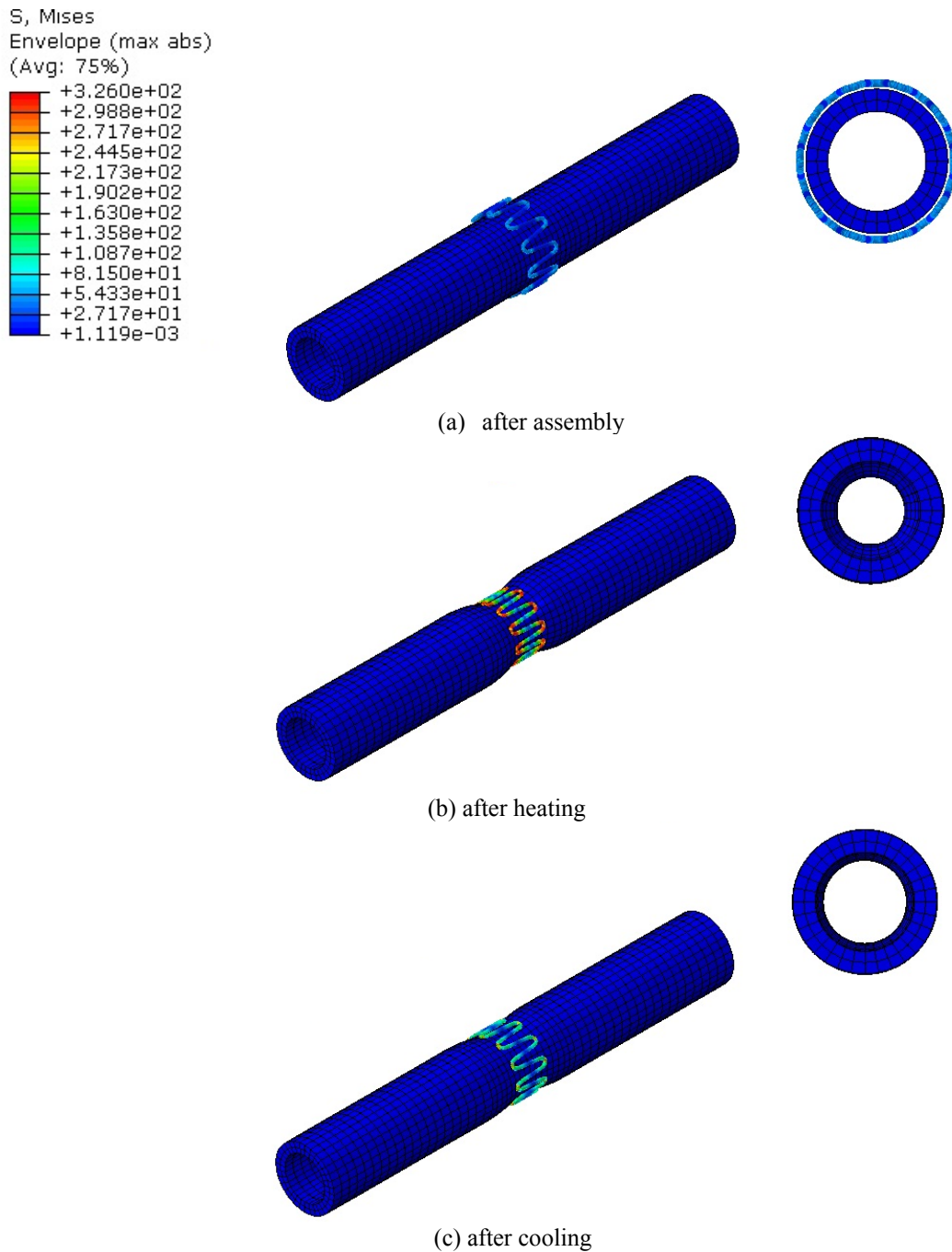


Fig. 13 Deformed shape and maximal von-Mises stress distribution (in MPa) in the SMA muscle and silicone rubber tube

We can notice that the stress of the artificial muscle reach its highest value in the folds areas. This is expected because the extension of the muscle is due to the unfolding of the pleats, which means that it is principally the areas that will be the most stressed. This implies that the martensitic transformation in these regions has been triggered, and a part or the entire SMA is converted into martensitic phase. This fact is confirmed by Fig. 12, showing the distribution of the volume fraction of martensite in the muscle.

After assembly of the two parts (Fig. 13(a)) and heating, the muscle contracts around the tube and applies a pressure in its outer surface as shown in Fig. 13(b).

After cooling the SMA artificial muscle to the assumed ambient temperature of 20°C, the simulation results show a relaxation of the muscle and as a result the tube (Fig. 13(c)). Indeed, after heating, a part of the volume fraction of martensite in the SMA artificial muscle disappears (Fig. 14) and is transformed into austenite.

Therefore, the portion of the strain associated with martensitic phase is transformed to an elastic strain which results in an increase in the stresses resulting in a radial force applied on the muscle in the direction of the recovery of its original shape. This force is transmitted by contact to the rubber tube thereby inducing a relatively considerable pressure on its outer surface sufficient to deform it (Fig. 15(a)).

As shown in Fig. 15(a) the average value of the pressure applied by the muscle on the rubber tube is in the order of 20000 Pa which is equivalent to a radial compressive force per unit length around the tube about of 200 N/m.

When the SMA temperature decreases the start stress of the austenite to martensite transformation decreases. Therefore, the stresses applied to the fold zones of the muscle have become greater than the critical stress for transformation from austenite to martensite σ_s^{AM} . This implies the onset of a new martensitic transformation accompanied by an important deformation due to martensite formation. This behaviour involves a decrease of the apparent rigidity of the muscle and induces its relaxation. The pressure applied to the tube becomes weak and relaxes (Fig. 15(b)).

In order, to investigate repeatability in the performance of the muscle, a series of heating and cooling cycles of the SMA wire were undertaken. As indicated before, energy was assumed to be provided by electric current. As can be seen from Fig.16 this has induced a cyclical contraction of the tube.

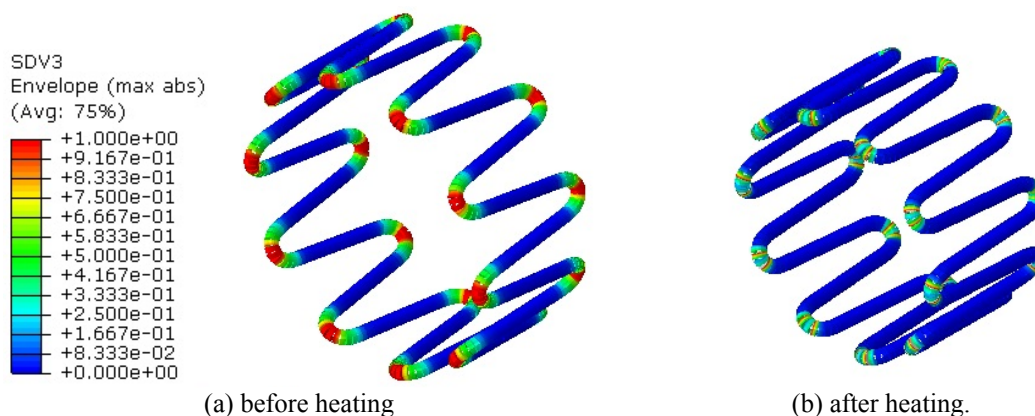


Fig. 14 Volume fraction of martensite

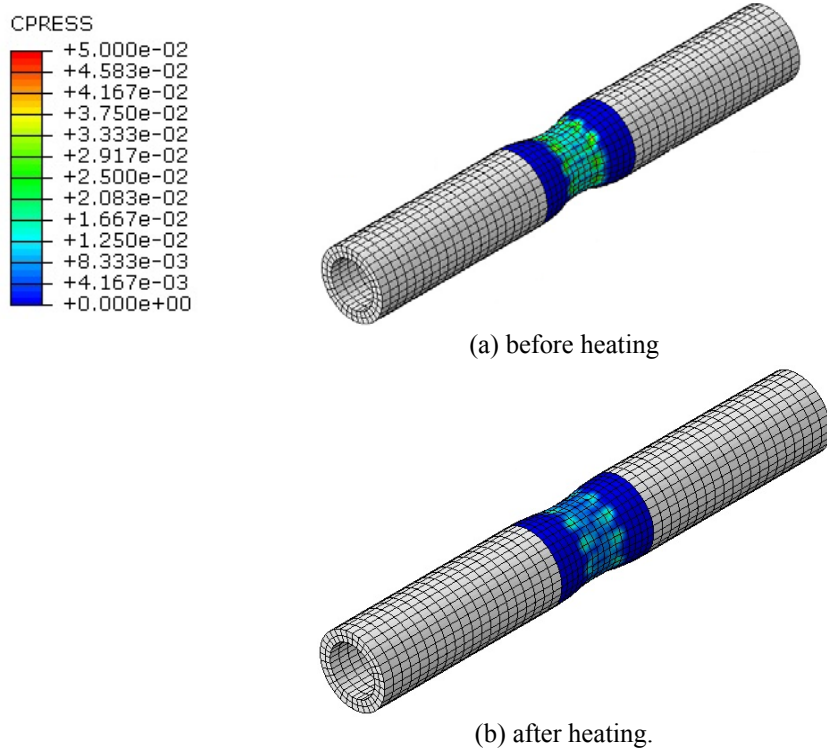


Fig. 15 Distribution of the pressure (in MPa) on the outer surface of the rubber tube

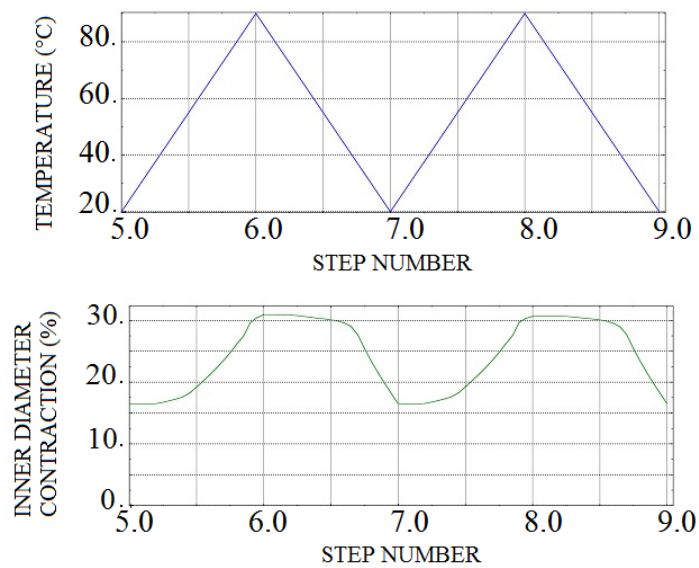


Fig. 16 Relative contraction of the inner diameter of the silicone rubber tube under cyclic heating and cooling

5. Conclusions

This paper presents a biomimetic artificial circular muscle designed to mimic the kinematic of natural circular muscle such as those located in small intestine. A new design based on SMA wire is proposed. A finite element analysis of the artificial muscle mounted around a silicone rubber tube has been conducted. To achieve this goal an SMA constitutive model is implemented in the commercial finite element software “Abaqus” using its customized subroutine “UMAT”. Simulation results show that, after properly selecting the design parameters, the new design is able to reproduce the natural circular muscle behaviour. This preliminary study has also demonstrated that the contraction/relaxation of the muscle can be controlled by heating using electric current. Experimental studies of the new muscle must be considered to provide a reliable assessment of the reliability and durability of this new design which will be investigated in our future work.

References

- Ali, A., Hosseini, M. and Sahari, B.B. (2010), “A review of constitutive models for rubber-like materials”, *Am. J. Eng. Appl. Sci.*, **3**(1), 232.
- Ben Jaber, M., Smaoui, H. and Terriault, P. (2008), “Finite element analysis of a shape memory alloy three-dimensional beam based on a finite strain description”, *Smart Mater. Struct.*, **17**(4), 045005.
- Brinson, L.C. and Huang, M.S. (1996), “Simplifications and comparisons of shape memory alloy constitutive models”, *J. Intell. Mat. Syst. Str.*, **7**(1), 108-114.
- Bundhoo, V. and Park, E.J. (2005), “Design of an artificial muscle actuated finger towards biomimetic prosthetic hands”, *In : Advanced Robotics ICAR'05 Proceedings, 12th International Conference on IEEE*.
- Dassault S. (2010), *Abaqus User Subroutines Reference Manual*, Woodland Hills, Canada.
- De Souza Neto, E.A., Peric, D. and Owen, D.R.J. (2011), *Computational methods for plasticity: theory and applications*, John Wiley & Sons.
- Dhatt, G., Touzot, G. and Cantin, G. (1984), *The Finite Element Method Displayed*, John Wiley & Sons Chichester, UK.
- Doroftei, I. and Stirbu, B. (2014), “Application of Ni-Ti shape memory alloy actuators in a walking micro-robot”, *Mechanics*, **20**(1), 70-79.
- Furst, S.J., Bunget, G. and Seelecke, S. (2013), “Design and fabrication of a bat-inspired flapping-flight platform using shape memory alloy muscles and joints”, *Smart Mater. Struct.*, **22**(1), 014011.
- Hartl, D.J., Lagoudas, D.C., Calkins, F.T. and Mabe, J.H. (2010), “Use of a Ni60Ti shape memory alloy for active jet engine chevron application: I. Thermomechanical characterization”, *Smart Mater. Struct.*, **19**(1), 015020.
- Lagoudas, D.C. (2000), *Shape Memory Alloys: Modeling and Engineering Applications*, Springer.
- Leary, M., Huang, S., Ataalla, T., Baxter, A. and Subic, A. (2013), “Design of shape memory alloy actuators for direct power by an automotive battery”, *Mater. Design*, **43**, 460-466.
- Lu, Z.K. and Weng G.J. (1994), “Martensitic transformation and stress-strain relations of shape-memory alloys”, *J. Mech. Phys. Solids*, **45**(11), 1905-1928.
- Luo, Y., Okuyama, T., Takagi, T., Kamiyama, T., Nishi, K. and Yambe, T. (2005), “Thermal control of shape memory alloy artificial anal sphincters for complete implantation”, *Smart Mater. Struct.*, **14**(1), 29.
- Madden, J.D., Vandesteeg, N.A., Anquetil, P.A., Madden, P.G.A., Takshi, A., Pytel, R.Z., Lafontaine, S.R., Wieringa, P.A. and Hunter, I.W. (2004), “Artificial muscle technology: physical principles and naval prospects”, *IEEE J. Oceanic Eng.*, **29**(3), 706-728.
- Mascaro, S.A. and Asada, H.H. (2003), “Wet shape memory alloy actuators for active vasculated robotic flesh”, *In : Robotics and Automation Proceedings. ICRA'03, IEEE International Conference on IEEE*.
- Nespoli, A., Besseghini, S., Pittaccio, S., Villa, E. and Viscuso, S. (2010), “The high potential of shape

- memory alloys in developing miniature mechanical devices: A review on shape memory alloy mini-actuators”, *Sensor. Actuat. A - Phys.*, **158**(1), 149-160.
- Orgéas, L. and Favier, D. (1998), “Stress-induced martensitic transformation of a NiTi alloy in isothermal shear, tension and compression”, *Acta. Mater.*, **46**(15), 5579-5591.
- Otsuka, K. and Wayman, C.M. (1999), *Shape Memory Materials*, Cambridge University Press.
- Patoor, E. and Berveiller, M. (1994), *Technologie des Alliages à Mémoire de Forme: Comportement Mécanique et Mise en Ouvre*, Hermes.
- Rediniotis, O.K. and Lagoudas, D.C. (2001), “Shape memory alloy actuators as locomotor muscles”, *Prog. Astronaut. Aeronaut.*, **195**, 483-500.
- Zienkiewicz, O. C. and Taylor, R. L. (2005), *The finite element method for solid and structural mechanics*. Butterworth-heinemann.